Energy & Environmental Science

COMMUNICATION

Electronic Supplementary Information for

All-region-applicable, continuous power supply of graphene oxide composite

Yaxin Huang,[a] Huhu Cheng,[a*] Ce Yang,[a] Houze Yao,[a] Chun Li,[b] and Liangti Qu[a,b,c*]

[a.] *Key Laboratory for Advanced Materials Processing Technology, Ministry of Education of China; State Key Laboratory of Tribology, Department of Mechanical Engineering, Tsinghua University, Beijing 100084, PR China. Email: lqu@tsinghua.edu.cn; huhucheng@tsinghua.edu.cn*
[b.] *Department of Chemistry, Tsinghua University, Beijing 100084, P. R. China.*
[c.] *School of Chemistry and Chemical Engineering, Beijing Institute of Technology, Beijing 100081, PR China.*

Methods

Synthesis of the GO composite.

Graphene oxide (GO) was synthesized by a modified Hummer's method reported previously[s1, s2]. Typically, 3 g graphite (325 mesh), 1.5 g sodium nitrate and 80 mL concentrated sulfuric acid (98 wt%) were mixed together and stirred in an ice bath for 30 min. Then, 18 g potassium permanganate was slowly added to this mixture, taking care to keep the temperature below 5 °C. Subsequently, the reaction mixture was transferred to a 35 °C water bath and stirred for 1 h. Then, 450 mL deionized water was carefully added and the solution was violently stirred for 30 min while raising the system temperature to 90 °C. Next, additional 500 mL deionized water was added, followed by the addition of 20 mL hydrogen peroxide (30 wt%) until the solution became orange brown. The resulting solution was filtered and washed with 200mL hydrochloric acid (3.7 wt%) overnight. The derived filter cake was dispersed in deionized water, with stirred overnight. Any unexfoliated graphite was removed by centrifuging the solution at 5000 rpm for 30 min twice with the precipitation discarded. Then, the dispersion was put into the dialysate bag (3000 Da) and dialyzed for a week to remove residual ions. The collected GO was diluted using deionized water to adjust the concentration for 5 mg mL^{-1}.

Sodium polyacrylate (PAAS, 10000 Da) was purchased from Beijing Chem. Reagents Co. (Beijing, China) and used as received. PAAS solution (2.7 mg mL^{-1}) was slowly added to GO solution (5 mg mL^{-1}) with vigorous stir, and the mixture was subjected to sonication for 30 min to obtain homogenous dispersions. The relative content of composite can be easily adjusted by changing the volume of PAAS solution. The blend (6 mL) was subsequently freeze-dried in a cylindrical polyethylene terephthalate container (5 mm in diameter) using commercial lyophilizer for 48 hours to get porous aerogel.

Fabrication of heterogeneous GO composite.

The heterogeneous GO composite membrane was fabricated by a two-step procedures. First, the freeze-drying porous aerogel was tableting under a pressure of 10 KN for 10 min to enhance the mechanic properties. The composite thickness was controlled by virtue of spacers with anticipative thickness while keeping the same pressure. Then, the membrane undergone unidirectional reduction in a custom-built device assisted with UV laser (15 W, 365 nm) using directionally-controlled laser irradiation methods developed in our recently work[s2]. Specifically, the GO/PAAS composite membrane was installed on a thermal-insulated plate, above which was the UV laser and a mask with hollowed pattern to mediate the focus of the laser. The reduction degree can be conveniently adjusted by variation of the reduction time. The sample was processed into rectangle shape with desired dimensions and consists of a moist-electric device with metal electrodes.

Electric measurement.

Electric measurements were performed with a Keithley 2612B multifunctional source meter. The samples were placed at ambient environment or in a homemade container with adjusted relative humidity by pumping mixture of dry and wet nitrogen. The testing temperature was adjusted by a hot plate or refrigerator. The circuit parameters of open circuit voltage test were current = 0 nA

and step index = 10 points s^{-1}. The circuit parameters of short circuit current test were voltage = 0 mV and step index = 10 points s^{-1}. The *I-V* characteristic was measured using electrochemical station CHI 660 sweeping voltages from -0.5 V to 0.5 V with the step voltage of 50 mV. The galvanostatic charge-discharge curves was measured using CHI 660 with a charge current density and discharge current density of 0 and 10 μA cm^{-2}.

Calculation of Schottky barrier height.

The Schottky barrier height can be calculated by *I-V* curves according to thermionic emission theory[s3], and the relationship between applied voltage and the current can be expressed as:

$$I = I_0 exp\left(\frac{qV}{nkT}\right)\left[1 - exp\left(\frac{-qV}{kT}\right)\right]$$

where I_0, q, n, k, T are the reverse saturation current, electronic charge, ideality factor, Boltzmann constant and temperature in Kelvin, respectively. For V>3kT/q, it can be simplified to

$$I = I_0 exp\left(\frac{qV}{nkT}\right)$$

the reverse saturation current can be extracted by extrapolating the straight line of lnI to intercept the axis at zero voltage

$$lnI = lnI_0 + \frac{q}{nkT}V$$

and the reverse saturation is also theoretically determined by

$$I_0 = AA^* T^2 exp\left(\frac{-q\varphi_b}{kT}\right)$$

where A, A^*, ϕ_b are the effective contact area, effective Richardson constant and zero-bias barrier height, respectively. Thus, the Schottky barrier height can be expressed as

$$\varphi_b = \frac{kT}{q} ln\left(\frac{AA^* T^2}{I_0}\right)$$

By plotting lnI–V curves, we can get the Schottky barrier height.

Calculation of the energy density.

The energy density of the MEG at different humidity and temperature conditions via galvanostatic discharge method. And the energy can be calculated by

$$E = I \times \int_0^t U$$

where I, U, t are the discharge current, the electric potential and discharge time, respectively. The volumetric energy density (E_v) and gravimetric energy density (E_m) can be expressed by

$$E_v = \frac{E}{Sh}$$

$$E_m = \frac{E}{\rho Sh}$$

where S, h, ρ represent the surface area, thickness, and density of the GO composite. The density of GO composite was measured as 1.2±0.1 g cm^{-3}.

Characterization.

Scanning electron microscopy (SEM) images were taken using a scanning electron microscope (SEM, FLexSEM 1000). X-ray diffraction (XRD) measurements were carried out using a Bruker AXS D2 PHASER diffractometer with a Cu Kα irradiation source (λ = 1.54 Å). X-ray photoelectron spectroscopy (XPS) was performed using a PHI Quantera II (Ulvac-Phi Incorporation) photoelectron spectrometer with Al Kα (1846.6 eV). Raman spectra were conducted using a LabRAM HR Raman spectrometer (Horiba Jobin Yvon) with a 532-nm laser. Fourier Infrared (FT-IR) spectra were collected using a UATR Two FT-IR spectrometer. Atomic force microscopic (AFM) images of flakes deposited on the silicate substrates were obtained in tapping mode using an Innova (Bruke) atomic force microscope. The contact angle of water droplets on GO composite was measured by an OCA25 Contact Angle meter (Dataphysics). The Zeta potential of samples was performed using Zetasizer Nano ZS (Malvern Panalytical). Theelectricsignals were recorded in real time using a Keithley 2612 multimeter controlled by a LabView-based data acquisition system. The environmental relative humidity and temperature were recorded by Center 313 Rs-232 Humidity Temperature Meter with a LabView-based data acquisition system.

Postmortem chemical component analysis.

The up and bottom surfaces of GO composite was firstly examined by EDS. Then, the GO composite was sandwiched by a pair of metal electrodes and connected with the external circuit at open circuit state for a long period (~6 h) to get equilibrium. The GO composite was further taken out to test the chemical component using EDS, recording the chemical content at the two surfaces. Afterwards, the sample was subsequently cut into three pieces (I, II, III). Sample I was discharging at short circuit state for ~6 h,

and the chemical content was investigated using EDS. Sample II and III were experienced discharge-charge and discharge-charge-discharge, respectively, and following checking the chemical content using EDS. All samples were testing at 25 °C, 60% RH.

Theoretical modeling.

The ionic migration induced electricity generation mechanism of moist-electric generator was analyzed by a theoretical model based on Nernst-Plank and Poisson equations (NPP)[s1, s4, s5] with proper boundary conditions

$$\nabla^2\varphi = -\frac{F}{\varepsilon}\sum z_i c_i$$

$$j_i = D_i(\nabla c_i + \frac{z_i F c_i}{RT}\nabla\varphi)$$

$$\nabla \cdot j_i = 0$$

where φ, F, ε, z, c, D, j, R and T are the electric potential, Faraday constant, dielectric constant, valence of ionic species, ions concentration, diffusion coefficient, ionic flux, ideal gas constant and temperature, respectively. The dielectric constant of the composite is estimated by considering the ratio of GO and PAAS with a linear relationship and it is heavily correlated with the relative humidity. The diffusion coefficients for carriers in the solid electrolyte are assumed 1.0×10^{-15} m^2 s^{-1}. The ion concentration of movable carrier is assumed as 2.2×10^{-8} mol L^{-1} and changed upon different relative humidity. The boundary condition for induced potential on the composite membrane surface is described by

$$\vec{n} \cdot \nabla\varphi = -\frac{\sigma}{\varepsilon}$$

where σ is the surface charge density that depends on the ionic concentration. The ions flux in steady state has the zero normal components at the boundaries

$$\vec{n} \cdot j = 0$$

Supplementary Figures

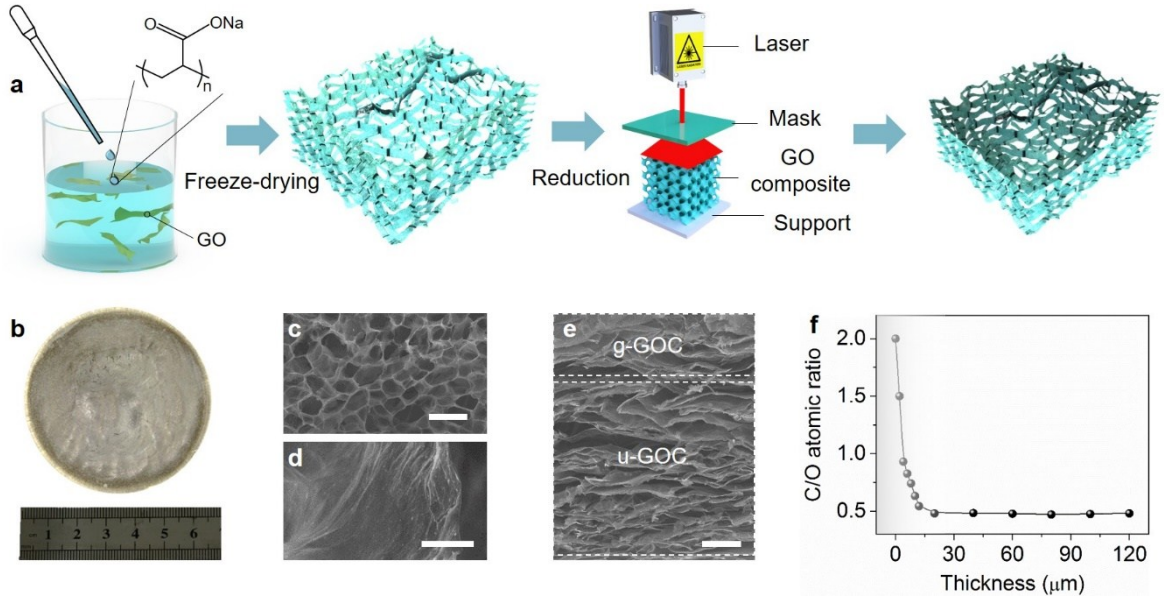

Fig. S1. Preparation and characterization of GO composite. (a) Preparation process of GO composite. (b) Optical photo of as-fabricated GO composite with a diameter of 6.5 cm and a thickness of 1 cm. (c) and (d) SEM images of GO composite at different magnification. It shows abundant micro pores and homogenous combination of polymers with GO sheets. (e) Cross-sectional SEM image of GO composite after directional reduction, composed of gradient reduced part (g-GOC) and unreduced u-GOC part. (f) C/O atomic ratio of GO composite along the cross-sectional direction in (e). Scale bars: c, 100 μm; d, 20 μm; e, 20 μm.

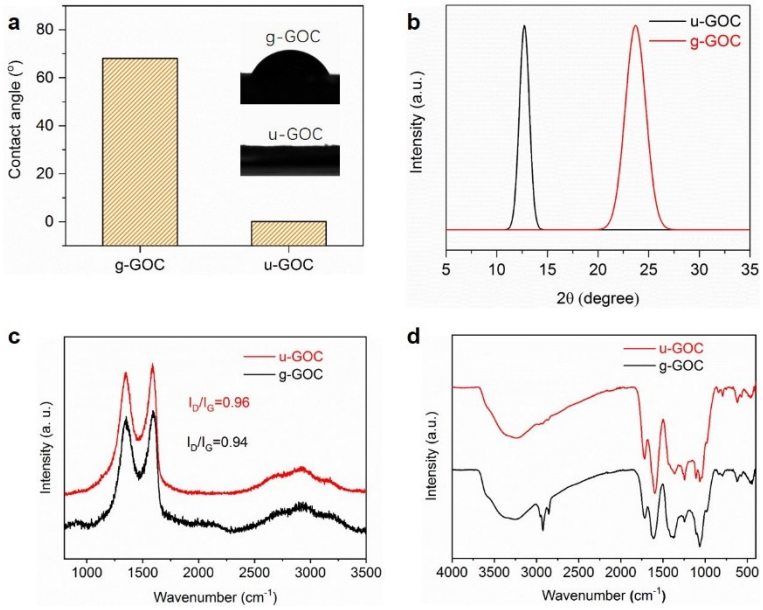

Fig. S2. **Chemical characterizations of GO composite.** (a) The contact angle of GO composite. The insets show the images of GO composite at reduced side (g-GOC, right up panel) and unreduced side (u-GOC, right bottom panel). (b) XRD patterns of u-GOC and g-GOC. (c and d) Raman and FT-IR spectrum of u-GOC and g-GOC.

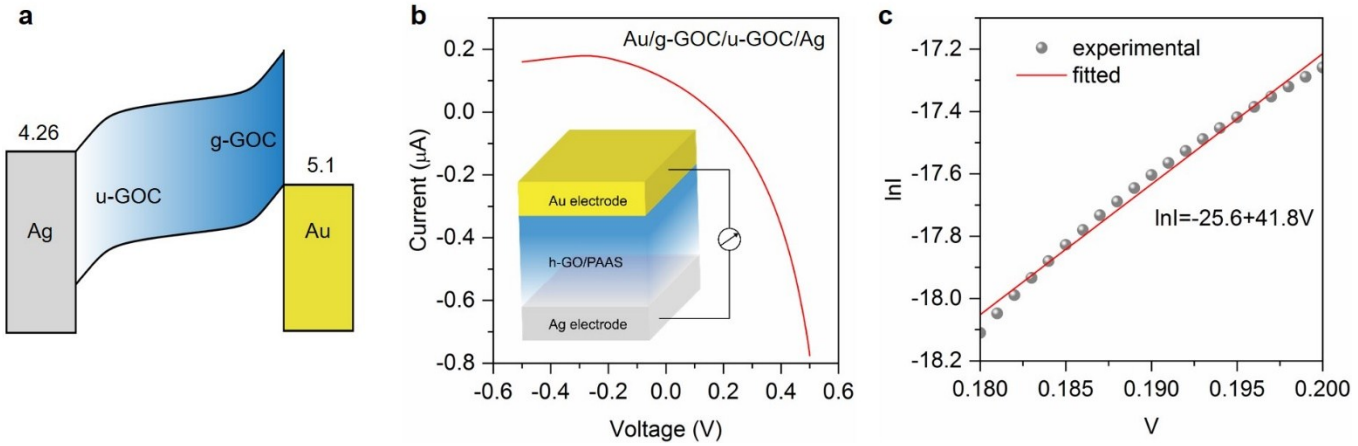

Fig. S3. **I-V characteristics of MEG.** (a) Energy band diagram of the MEG. (b) I-V curves of the moist-electric generator with a device configuration of Au/gGOC/u-GOC/Ag. (c) lnI versus V plot extracted from (b).

According to the semiconductor theory[s6], the contact between metal and semiconductor can be categorized to Ohmic and Schottky contacts, which are dependent on the band structure of metal and semiconductor. An apparent characteristic of Ohmic contact is the non-rectifying electric behavior that has a linear current–voltage (I-V) curve as with Ohm's law. By contrast, the Schottky contact demonstrates a rectifying characteristic along with a non-linear I-V curves.

In the MEG regime, Ag (4.26 eV) has a lower work function than u-GOC (4.9 eV[s7]), which can form a prominent Schottky junction at the Ag/u-GOC interface. While the Au (5.1 eV) has a higher work function than g-GOC (4.4–4.7 eV[s7–s9]), thus forming an Ohmic contact at the Au/g-GOC interface. As illustrated in Fig. S3b, the I-V curve of Au/g-GOC/u-GOC/Ag MEG displays a typical rectifying characteristic, where the current shows a non-linear feature at forward applied voltage and a linear feature at backward applied voltage, respectively. These results further confirm the Schottky contact characteristic at the Ag/u-GOC interface and Ohmic contact behaviour at the Au/g-GOC interface, consistent with the above analysis and previously reported literatures[s2, s10, s11]. From the lnI–V curves, we can get the Schottky barrier height at Ag/u-GOC interface to be 0.064 eV.

The GO composite has numerous oxygen functional groups bonded to the carbon plane, such as C–O and C=O, where the O atom tends to pull electrons from the C atom, leaving a hole in the carbon network. This results in p-type semiconductor behaviour of GO composite, with the carrier concentration difference dependent upon the degree of oxidation. Therefore, both the u-GOC and g-GOC are p-type semiconductor, consist with previously reported literatures[s7, s12].

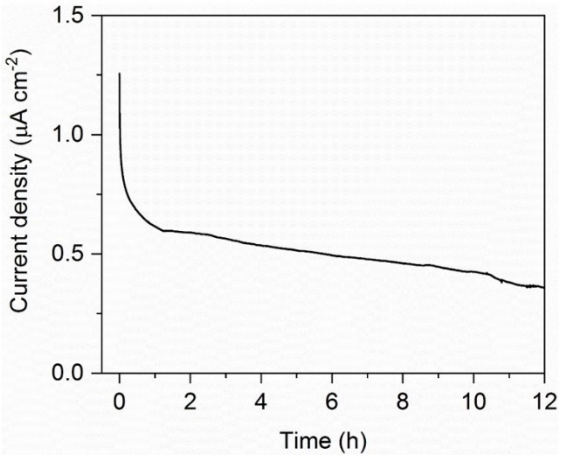

Fig. S4. Short circuit electric current output of MEG.

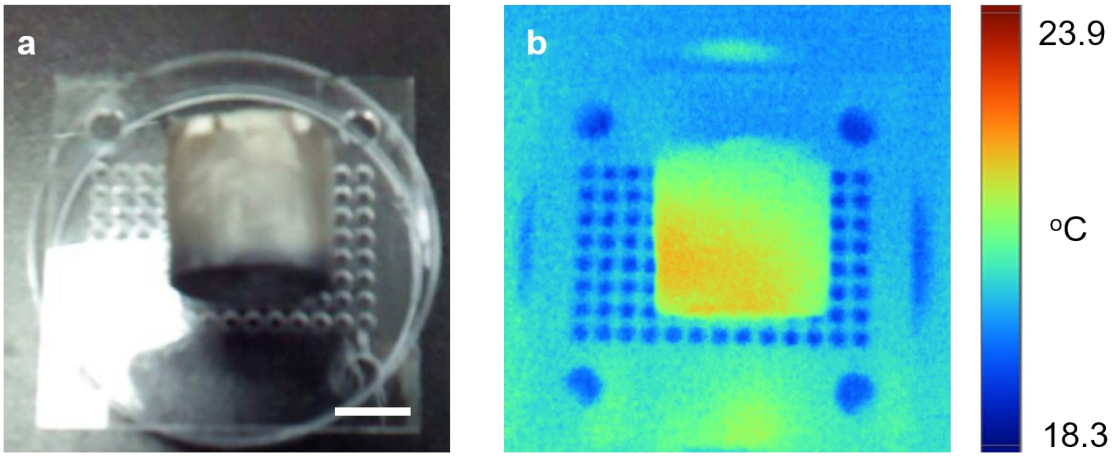

Fig. S5. **Evaluation of moisture distribution across GO composite.** (a) and (b), optical image and infrared thermal imaging photos of GO composite placed above a water container. Scale bar: 1 cm. The water container was utilized to facilitate the adsorption of water molecules onto GO composite and served as a cool background for contrast. Generally, the object's temperature would decrease, after absorbed with water molecules. Therefore, we can simply evaluate the water molecules distribution in the GO composite via infrared thermal imaging. The infrared thermal imaging photo of GO composite shows distinct temperature difference, in which the g-GOC side shows a higher temperature while u-GOC side shows a lower temperature, indicating an absorbed moisture difference. It should be noted that the temperature difference across GO composite was not changed with time evolution.

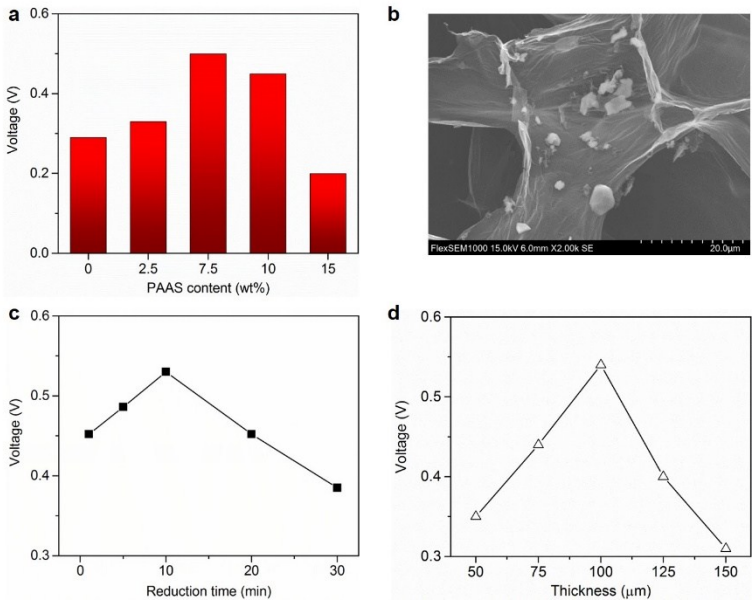

Fig. S6. **Output performance optimization of MEG.** (a) Voltage output of GO composite with different PAAS weight content tested at room temperature and 30% RH. (b) SEM images of GO composite with polymer content of 15%. It shows aggregation of polymers. (c) Voltage output of GO composite with different laser reduction time tested at room temperature and 30% RH. (d) Voltage output of GO composite with different device thickness tested at room temperature and 30% RH.

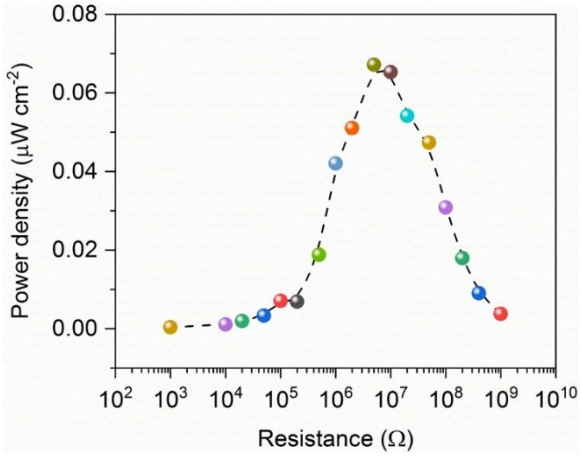

Fig. S7. Power density of MEG with different electric resistors.

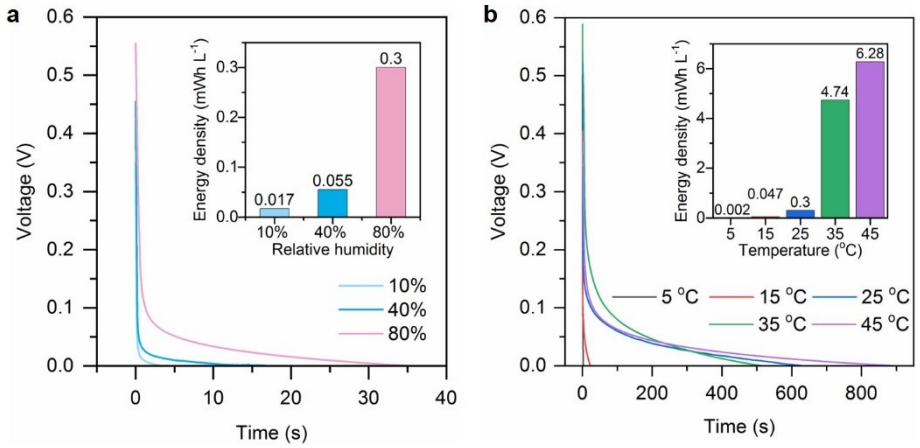

Fig. S8. Galvanostatic discharge curves of the MEG at (a) different humidity and (b) various temperature. The discharge current density is 10 μA cm^{-2}. The inset shows the calculated volumetric energy density of the MEG.

The energy density remarkably increases with increased relative humidity and realizes the highest volumetric energy density of 0.3 mWh L^{-1} and gravimetric energy density of 0.25 mWh Kg^{-1} at 80% environmental humidity. Higher humidity would promote the adsorption of moisture on the GO composite, giving rise to more moveable carriers and beneficial for its transport. Furthermore, the energy density also exhibits an exceptional increase with incremental temperature, arriving a maximum volumetric energy density of 6.28 mWh L^{-1} and gravimetric energy density of 5.23 mWh Kg^{-1} at 45 °C, which should be attributed to the enhanced ionic conductivity of the GO composite at high temperature.

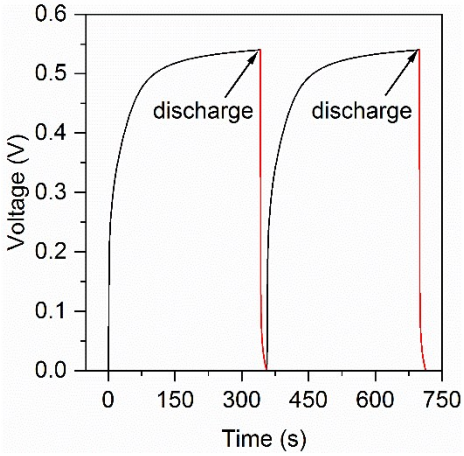

Fig. S9. Charge-discharge curves of the moist-electric generator. The charge process was spontaneously proceeded and a current density of 10 μA cm^{-2} was applied for the discharge process. The sample is tested at room temperature with a relative humidity of 80%.

To evaluate the energy recharged by autonomously adsorption of moisture form environment, a spontaneous charge-initiative discharge electric measurement was conducted on the MEG. Typically, the MEG was connected with electrochemical station in galvanostatic charge/discharge mode, the charge and discharge current density was set as 0 and 10 μA cm^{-2}, respectively. As shown in Fig. S9, the charged energy induced by autonomously adsorption of moisture from environment is 0.40 μJ via calculating the galvanostatic discharge curves. The recharge process needs a time of 343 s by adsorbing moisture from environment, and the recharged energy is 0.385 μJ. The slightly decreased recharged energy should be attributed to the weakened moisture adsorption capability induced by the thermal effect at the discharge process, which is similar to the discharge situation in other energy storage device (Li ions batteries and supercapacitors)[s13, s14].

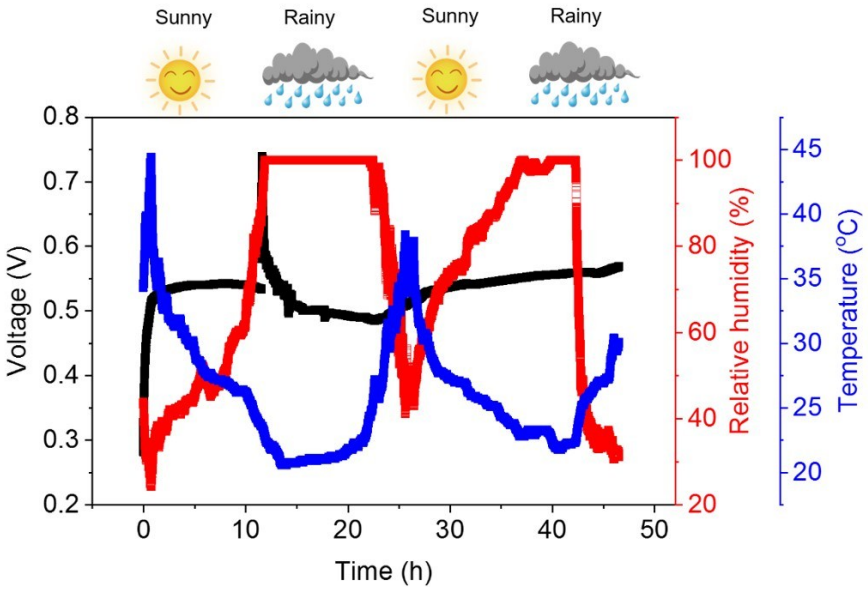

Fig. S10. The real-time recording voltage signal of MEG versus corresponding relative humidity and temperature evolution in different weather. Date: 30 Aug to 1, Sep, 2018, location: Campus of Tsinghua University, Beijing, China.

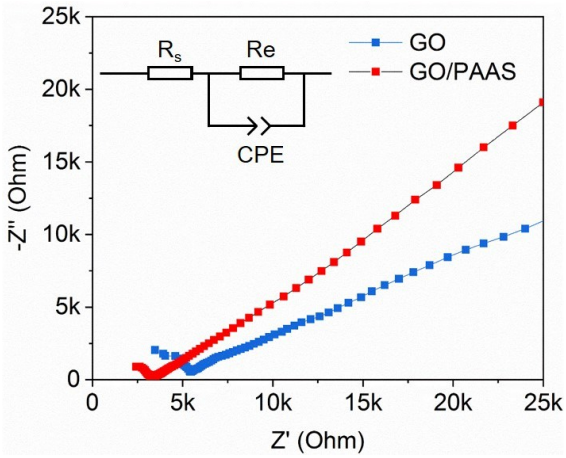

Fig. S11. EIS measurement of GO and GO/PAAS composite. The inset is the equivalent electric circuit.

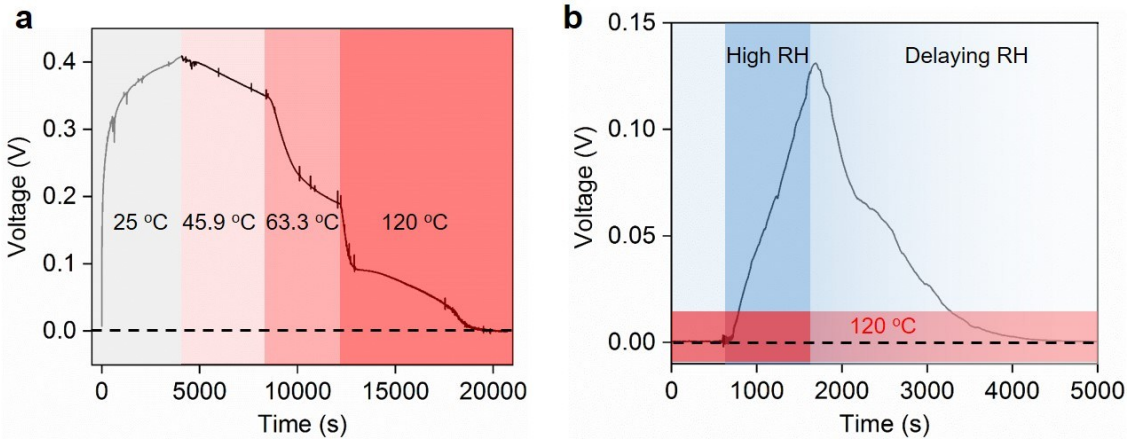

Fig. S12. (a) The voltage output of MEG upon sequential increased environmental temperature. The voltage is gradually decreased to zero at a high temperature of 120 °C, where the absorbed water molecules is fully removed from GO composite. (b) The voltage change of MEG with external applied moisture at 120 °C environment. The voltage is gradually increased with exposed high relative humidity and subsequently decreases to zero with delaying relative humidity. The results indicate that the water molecules inside GO composite due to the spontaneous absorption process is the basic reason for the occurrence of constant voltage of MEG.

Supplemental Reference

s1. H. Cheng, Y. Huang, F. Zhao, C. Yang, P. Zhang, L. Jiang, G. Shi and L. Qu, *Energy Environ. Sci.*, 2018, **11**, 2839-2845.
s2. Y. Huang, H. Cheng, C. Yang, P. Zhang, Q. Liao, H. Yao, G. Shi and L. Qu, *Nature Communications*, 2018, **9**, 4166.
s3. E. Rhoderick, R. Williams and M. S. Contacts, *Journal*, 1988.
s4. W. Guo, Y. Tian and L. Jiang, *Accounts of chemical research*, 2013, **46**, 2834-2846.
s5. J. Gao, W. Guo, D. Feng, H. Wang, D. Zhao and L. Jiang, *Journal of the American Chemical Society*, 2014, **136**, 12265-12272.
s6. C. Henry, *IEEE Journal of Quantum Electronics*, 1982, **18**, 259-264.
s7. J. Liu, M. Durstock and L. M. Dai, *Energy Environ. Sci.*, 2014, **7**, 1297-1306.
s8. H. M. Huang, Z. B. Li, J. C. She and W. L. Wang, *J. Appl. Phys.*, 2012, **111**, 4.
s9. A. Mathkar, D. Tozier, P. Cox, P. J. Ong, C. Galande, K. Balakrishnan, A. L. M. Reddy and P. M. Ajayan, *J. Phys. Chem. Lett.*, 2012, **3**, 986-991.

s10. M. Dragoman, G. Deligeorgis, A. Muller, A. Cismaru, D. Neculoiu, G. Konstantinidis, D. Dragoman, A. Dinescu and F. Comanescu, *J. Appl. Phys.*, 2012, **112**, 4.
s11. M. R. Islam, D. Joung and S. I. Khondaker, *New J. Phys.*, 2011, **13**, 10.
s12. D.-T. Phan and G.-S. Chung, *Journal of Physics and Chemistry of Solids*, 2013, **74**, 1509-1514.
s13. B. M. Schumacher, *Journal of Materials Processing Technology*, 2004, **149**, 376-381.
s14. W. Pell, B. Conway and N. Marincic, *Journal of electroanalytical chemistry*, 2000, **491**, 9-21.